European MSc in Marine Environment and Resources
UPV/EHU–SOTON–UB-ULg

Erasmus Mundus
REF: 2013-0237

Analysis of the effect of Medicane Ianos on Sea Surface Temperature in Ionian Sea

---

A thesis submitted in partial fulfillment

of the requirements for the degree of

Master of Sciences

By:

Kenechukwu Francis Uba (MER+ 2019-2021)

Supervisor:

Dr. Aida Alvera Azcárate

(Researcher at the University of Liège, Belgium)

September 2021

PLENTZIA (UPV/EHU), SEPTEMBER 2021

université de BORDEAUX

UNIVERSITY OF Southampton

eman ta zabal zazu
Universidad del País Vasco
Euskal Herriko Unibertsitatea

LIÈGE université

Dr Manu Soto,
as teaching staff of the MER+ Master of the University of the Basque Country

CERTIFIES:

That the research work entitled "*Analysis of the effects of Medicane Ianos on Sea Surface Temperature in the Ionian Sea*" has been carried out by Kenechukwu Francis Uba at the University of Liege, Belgium under the supervision of Dr. Aida Alvera Azcárate from the University of Liege, to achieve 30 ECTS as a part of the MER+ Master program.

In…....……., September ……. 2021

Presenter:
Manu Soto

Supervisor:
Aida Alvera Azcárate

Sign.

Sign.

Acknowledgements

I would like to acknowledge everyone who played critical roles in helping me get to the end of this phase. In the first place, the coordinators of the MER+ program Ionan Marigomez and Manu Soto, Jorg Schäfer, and Maria Pílar Rodriguez, Maria Jímenez Garcia, Feli Olivares and Carlos at the MER Secretariat, and Isabelle Noirot at Uliège International Office. I also wish to thank my supervisor Dr. Aida Alvera-Azcárate, and the members of the GHER Research group at University of Liège including Dr. Alexander Barth, Prof. Jean-Marie Beckers, Charles Troupin and Bekti Mujiasih as well as fellow Master's student Cécile Pujol for their suggestions and helpful comments. I also appreciate all my lecturers from U-Bordeaux, UPV/EHU and ULiège.

A special thanks goes to Manal Hamdeno for her patient explanations and key suggestions at different times and for other numerous kindnesses. Thanks also to Soumaïa Tajouri, Priyanka Soni, Makanjuola Akinyemi, Gourab Chowdhury, Piyumi Kshanika, Nellie Wullenweber and all my classmates.

Lastly I appreciate the encouragement of my family and friends, in particular my parents, my brothers and sisters, and Fr. Chike Uba for all the cheering and prayers. May God bless you all.

Table of Contents

List of Figures:

List of Tables:

Abstract

The Mediterranean Sea is known for extratropical cyclones but occasionally under certain conditions cyclones that have tropical characteristics may be formed. These storms resemble tropical cyclones in some key features such as the presence of a storm ‘eye’, cloud walls and high winds and can have an impact both on coastal regions and in the ocean layer. In this work a tropical-like cyclone (also called Mediterranean hurricane or “medicane”) that occurred in September 2020 was examined. This medicane, which was named Ianos, began as a tropical low pressure system and intensified into a medicane within the Ionian Sea. DINEOF (Data INterpolating Empirical Orthogonal Functions) was used to reconstruct missing data due to cloud contamination. Satellite, reananlysis and in-situ data were used to examine the hydrographic effects of the medicane. The medicane led to the cooling of the SST by up to 4°C, deepening of the MLD by ~12m, increase in Chl-a concentration by an average of 0.07 mg/m³. Average heat loss to the atmosphere during this period was about -150 W/m². Medicane Ianos was accompanied by high winds and maximum gusts of up to 100 km/h around the Ionian islands making it a Category 1 Hurricane according to the Saffir-Simpson Scale. Salinity increase in the subsurface waters was observed following the medicane which was associated with horizontal advection and vertical mixing leading to the weakening of the Atlantic Water signal and the dominance of the Levantine Surface Water in this zone.

Résumé

La mer Méditerranée est connue pour ses cyclones extratropicaux, mais il arrive que, dans certaines conditions, des cyclones présentant des caractéristiques tropicales se forment. Ces tempêtes ressemblent aux cyclones tropicaux par certaines caractéristiques clés telles que la présence d'un "œil" de tempête, de murs de nuages et de vents violents et peuvent avoir un impact à la fois sur les régions côtières et dans la couche océanique. Dans ce travail, un cyclone de type tropical (également appelé ouragan méditerranéen ou "medicane") survenu en septembre 2020 a été examiné. Ce medicane, qui a été nommé Ianos, a commencé comme un système tropical de basse pression et s'est intensifié en medicane dans la mer Ionienne. DINEOF (Data INterpolating Empirical Orthogonal Functions) a été utilisé pour reconstruire les données manquantes dues à la contamination des nuages. Des données satellitaires, de réanalyses et in-situ ont été utilisées pour examiner les effets hydrographiques de la medicane. La medicane a conduit à un refroidissement de la SST jusqu'à 4°C, à un approfondissement du MLD de ~12m, à une augmentation de la concentration de Chl-a d'une moyenne de 0.07 mg/m³. La perte moyenne de chaleur vers l'atmosphère pendant cette période était d'environ -150 W/m². Medicane Ianos a été accompagné de vents violents et de rafales maximales de 100 km/h autour des îles Ioniennes, ce qui en fait un ouragan de catégorie 1 selon l'échelle de Saffir-Simpson. Une augmentation de la salinité des eaux de subsurface a été observée à la suite du medicane, associée à une advection horizontale et à un mélange vertical conduisant à l'affaiblissement du signal des eaux atlantiques et à la prédominance des eaux de surface levantines dans cette zone.

1. Introduction

The Intergovernmental Panel on Climate Change (IPCC) Special Report on the Ocean and Changing Cryosphere (SROCC) gives a definition of extreme weather/climate events as one “that is rare at a particular place and time of the year (Collins et al., 2019).” It goes further to say that “when a pattern of extreme weather persists for some time, such as a season, it may be classed as an extreme climate event, especially if it yields an average or total that is itself extreme (Collins et al., 2019).” Extreme events can have different impacts on the environment. When the other series of expected or unexpected impacts result from the occurrence of an extreme hazard such that there is a disruption of physical, natural, social or economic activities with larger effect than the initial impact then this can be classified as cascading impacts (Collins et al., 2019).

In the recent years, extreme weather events that have been identified include marine heat waves (MHW), droughts, wave-induced flooding, extreme rainfalls and cyclones. These events can occur either singly or as compound events occurring due to multiple drivers (Collins et al., 2019). For example, in the North Atlantic, in 2005 there was a record number of tropical storms and hurricanes which was linked to the trend in SST, the previous El Niño and the Atlantic Multidecadal Variability (AMV) (K. E. Trenberth & Shea, 2006). One of the hurricanes was Hurricane Katrina which led to over 1800 deaths and about 30 billion USD in losses (Link, 2010). In the Northeast Pacific Ocean, between 2013–2015, the largest heatwave was recorded with temperatures up to 6°C above normal (Jacox et al., 2016; Rudnick et al., 2017). This MHW induced the outbreak of a toxic algal bloom along the US West coast that impacted the fisheries (McCabe et al., 2016) and increased sea bird mortality (Jones et al., 2018) These are a few examples of extreme weather events that are linked to either anthropogenic or natural influences.

1.1 Tropical Cyclones

Cyclones occur in different oceans and seas as a result of atmospheric dynamics that are linked to differences in air pressure. When viewed as extreme events, the reference is to cyclones and storms that are rare within the given area. The rarity may linked to the intensity of the occurrence or the number of unique occurrences. Among the cyclones that rank as extreme weather events are the tropical cyclones.

Tropical cyclones refer to non-frontal low-pressure systems that occur over tropical or subtropical waters with organised convection and definite cyclonic surface wind circulation (Henderson-Sellers et al., 1998). Tropical cyclones are associated with very low pressure, and based on maximum sustained wind speed (i.e., the Saffir-Simpson scale), tropical cyclones are grouped into tropical depressions, tropical storms and category 1 to category 5 hurricanes with increase in wind speed (Wang, 2015). A storm with surface winds up to 33 ms^{-1} is called a “typhoon” in the Northwest Pacific Ocean, a “hurricane” in the North Atlantic and northeast Pacific Oceans, or a “severe tropical cyclone” in the southwest Pacific and southeast Indian Oceans (Neumann, 1993). The energy for tropical cyclones is derived mainly from evaporation from the ocean and the condensation in convective clouds that is found near their centre (Holland, 1993). Another characteristic of tropical cyclones is the presence of a “warm core” in the troposphere that is relatively warmer than the environment at the same pressure level (Henderson-Sellers et al., 1998). This warm-core is responsible for the strong surface winds associated with tropical cyclones that induce storm surge, wave action and damages to coastal regions (Emanuel, 2005)(Anthes, 1974).

Tropical cyclones are also seasonal events occurring mostly in the late summer to early autumn period as this is the period of maximum sea surface temperature (SST) as one of the factors driving the formation of the cyclones. In the North Atlantic, the storm season is between August to October with maximum frequency of occurrence in September (Neumann et al., 1985). According to Gray (1981), six environmental factors are related to the genesis of tropical cyclones:(i) large values of low-level relative vorticity, (ii.) Coriolis parameter a few degrees poleward of the equator, (iii.) weak vertical shear of horizontal winds, (iv.) high SST exceeding 26°C and deep thermocline, (v.) conditional instability through a deep atmospheric layer, and (vi.) large values of relative humidity in the lower and mid-troposphere.

1.2 Cyclones in the Mediterranean Sea

The weather in the Mediterranean is marked by an abundant sunshine as well as subtropical and mid-latitude systems which is influenced by the mountain ranges in the north. The Mediterranean Sea is acknowledged as a top cyclogenetic area with strong winds and heavy precipitation weather impacts that have a cyclonic signature (Horvath

et al., 2004; Tous & Romero, 2013). The size of these cyclones vary from synoptic to mesoscale, while the type of the differs from baroclinic to orographic or diabatically-modulated systems. In any case, it has been observed that their peak occurrences are linked to the presence of mountain ranges that surround the Mediterranean sea (Mastrantonas et al., 2021; Tibaldi & Buzzi, 1983). As a result, the countries in the Mediterranean region experience extreme weather impacts (Tous & Romero, 2013). Being a mid-latitude system, the cyclones draw their energy from horizontal temperature gradients in the atmosphere rather than the evaporation from the ocean which is the case in tropical cyclones (Henderson-Sellers et al, 1998). In addition, the cyclonic systems that occur in the Mediterranean are extratropical due to the presence of upper-level winds resulting from the difference in temperature between the equator and the poles. Notwithstanding this, one still finds cyclonic events that can be classified as 'meteorological bombs' (Homar et al., 2002).

These "meteorological bombs" are referring to the occasional cyclones that have tropical-like characteristics. They are a kind of polar low pressure systems that induce sudden changes in pressure and wind over the affected area (Trigo et al., 1999) although the winds may not always attain hurricane intensity (Tous et al., 2013). This kind of cyclone appears about thrice every two years (Nastos et al., 2018) and has been named the Mediterranean hurricanes or "medicanes" (Tous et al., 2013). When viewed from satelllite imagery, they are characterised by almost axisymmetric and deep warm-core structures, deep convective clouds and circular eyes surrounded by eyewalls (Miglietta & Rotunno, 2019; Pytharoulis et al., 2000).

The formation of medicanes occur when an upper-troposphere trough cutoff introduces cold air masses over the warm Mediterranean sea (Pytharoulis et al., 2018; Tous & Romero, 2013, Cavicchia et al., 2014). In addition, air-sea heat and moisture exchanges interact with the upper-air conditions and when there is an excess of heat and moisture in the lower troposphere due to the interactions between the baroclinic environment and the diabatic processes (Cavicchia et al., 2014), it triggers an atmospheric instability that is supported by the presence of weak vertical wind shear and high vorticity (Anthes, 1974).

For a cyclonic disturbance to be classified as a medicane, it needs to meet some criteria. First, they must possess a highly symmetric structure that is similar to that in tropical cyclones. They should also have a continuous cloud cover and the symmetric shape around the cyclone eye should remain visible. The diameter of the medicane is restricted to less than 300 km since the heat fluxes cannot create larger cyclones owing to the size of the Mediterranean sea. Lastly, the cyclone should have lasted at least 6 hours (Cavicchia et al., 2014b; Tous & Romero, 2013).

Although the two preferred regions of cyclogenesis are the Italian maritime areas, and the Ionian and Aegean seas, most of the medicanes have occurred over the Ionian and the Balearic seas (Tous & Romero, 2013, Nastos et al., 2018). In addition, notwithstanding that the Eastern Mediterranean (EMED) has warmer temperatures than in the Western Mediterranean (WMED), the presence of colder air arriving from central and northern Europe over the WMED makes it more susceptible to the formation of medicanes (Cavicchia et al., 2014a; Kassis & Varlas, 2021). The occurrence of medicanes during the year is also seasonal as the majority of the medicanes were observed in winter and autumn (Nastos et al., 2018; Tous & Romero, 2013).

The growth and maturation of a medicane thus depends on the complex interaction between the warm sea surface and cold upper-air. Other features like evaporation of the surface water, the sea-air heat exchanges, wave generation, upwelling and upper-layer mixing lead to a cooling which in turn create a negative feedback on the intensity of the medicane. Eventually, they not only influence the intensity but also the direction of the medicane (Tous et al., 2013a) since it has sufficient energy to travel hundreds of kilometers until it makes landfall while accompanied by strong winds and high precipitation and rainfall that cause floodings, and even landslides in some places (Kassis & Varlas, 2021; Varlas et al., 2020).

Whereas extratropical cyclones are baroclinic in origin and get their energy supply from the potential energy associated to the horizontal temperature gradients (Pytharoulis et al., 2018), the medicanes derive their energy from thermodynamic disequilibrium between the ocean and the atmosphere. As there is a huge release of latent heat in the clouds which is also moistened by the evaporation, the medicanes take a resemblance to tropical

cyclones (Tous et al., 2013a). In addition, medicanes do not develop by themselves, but rather require a large-scale disturbance like a cyclonic storm that is traveling over the Mediterranean to develop in its late or mature stages (Emanuel, 2005). They form generally under deep, cut-off cold core cyclones present in the upper and middle troposphere that had themselves formed from a synoptic-scale Rossby wave (Pytharoulis et al., 2000; Tous & Romero, 2013), and since cold cores are common in the Mediterranean whereas medicanes are rare, it suggests that there are other meteorological conditions that also come into play in the formation of the medicanes.

SST around 15ºC is about the minimum for a cyclone to form (Nastos et al., 2018). The presence of warm surface waters combined with cold air at upper levels lead to the thermodynamic disequilibrium described earlier. Although the minimum SST to produce a hurricane or tropical cyclone is at about 26ºC (Henderson-Sellers et al., 1998; K. Trenberth, 2005), one does not find these temperatures except in the southern Mediterranean during summer and so the medicanes can form at temperatures below 26ºC (Tous & Romero, 2013; Varlas et al., 2020).

1.3 History of Medicanes in the Mediterranean Sea

The size of the Mediterranean Sea is small compared to other oceans where cyclones occur. Consequently, medicanes often make landfall with impacts that include flooding, landslides, and heavy precipitation and rainfall on the coastal areas. This makes it important to know how to identify them in advance and issue early warnings as having an understanding of the characteristics and the atmospheric conditions that surround it is necessary to prepare for its impacts when it happens.

In the past, several storms have occurred in the Mediterranean Sea that looked like tropical-like cyclones. Efforts have been made to have a better understanding of the mechanisms behind the medicanes. Since it is a rare occurrence, studies have had to rely on historical data from satellite imagery combined with models to increase the recognition of the medicanes. Table 1 gives 15 of those storms that have been recognised as clearly meeting the criteria to be classified as medicanes. The first 14 were taken from Miglietta et al., (2013), and the last one was taken from Kassis &Varlas, (2021).

Table 1. Case studies of cyclones that showed tropical features with dates, minimum pressure, and wind speeds. (1-14 adapted from Miglietta et al., 2013;15. Kassis & Varsas, 2020)

	Area	Date	Min Pressure (hPa)	Max winds (m/s)
1	Ionian	13-09-1999	1007	23
2	Sicily	10-11/09/2000	1006	22
3	SE Italy	26/09/2006	980	45
4	Ionian	04/12/2008	990	42
5	S Italy	13-14/04/2012	982	39
6	Ionian	19/09/2004	1005	26
7	Sicily Strait	03-06/11/2004	1000-1005	30-24
8	Aegean Sea	09/10/2000	1000	24
9	Libya-Crete	13-15/12/2005	996-986	40-26
10	West Sardinia	27/05/2003	1000	30
11	Balearic Islands	17-18/10/2003	990	42
12	Balearic Islands	17/10/2007	1011	24
13	S France	26/10/2007	996	38
14	Balearic Islands /S France	06-08/11/2011	990	46
15	Ionian-Aegean seas	28-30/09/2018	990	33.5

1.4 Study Aims and Objectives

This work is aimed at studying a medicane that occurred in the Central Mediterranean Sea in September 2020. The medicane which was named “Ianos” by the Hellenic National Meteorological Service (HNMS) began as a storm on September 14, 2020 in the Gulf of Sidra at the North African coast and then travelled northeast into the Ionian sea where it acquired tropical characteristics by September 17th 2020.

The first objective is to calculate cloud-free SST from L3 satellite images using an interpolation technique known as DINEOF (Data Interpolating Empirical Orthogonal Functions) and then use the reconstructed data to study the impact of Medicane Ianos from the SST field. The second objective is to study the effect of Ianos on the SST, atmospheric parameters, and hydrographic structure of the central Mediterranean. Finally, this work aimed to study the effect of the medicane on the sea surface productivity.

2. Data and Methods of Analysis

2.1 Study Area

The major study area was designated as the Central Mediterranean Sea which lies between 15ºE–23ºE of longitude, and 32ºN – 42°N of latitude because the lifetime of the medicane Ianos occurred within the Ionian Sea. As stated earlier the Ionian Sea is also a site of several medicanes in the past. Within this large study area, several points were selected for a closer analysis of the effects based on the availability of in-situ data from Argo profiles. The track of the medicane (Figure 1) was plotted using Ianos' positions from the UK Met Office surface analysis maps

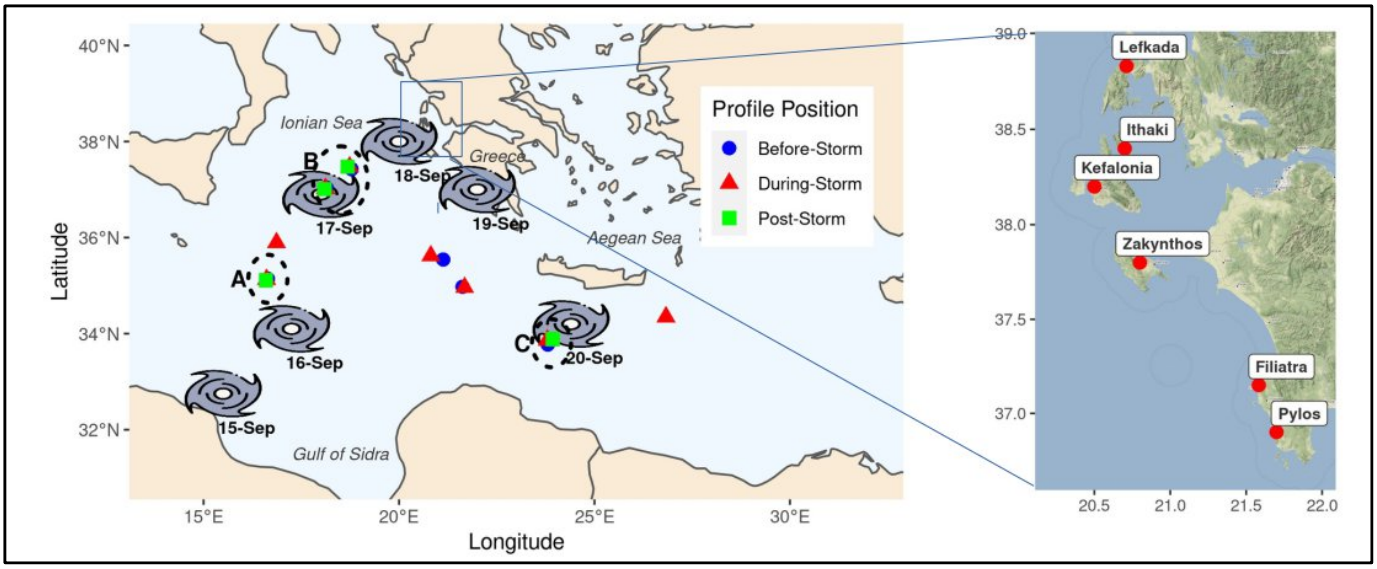

(https://www.metoffice.gov.uk/weather/maps-and-charts/surface-pressure).

Figure 1. Map of the study area showing the locations of Medicane Ianos at 00 UTC each day. Coloured points show the positions of the floats around the period of the medicane. A, B, C represent the groups of Argo profiles studied for the effects of the medicane.

2.2 Data

2.2.1 *Oceanographic remote sensed satellite data*

In order to study the oceanographic impacts of the medicane, the sea surface temperature (SST) was examined. The mean sea level pressure, air temperature, wind

speeds and sea surface height were also among the parameters studied from remote sensing and satellite data sources. Sea surface temperature (SST) influences the atmosphere through surface energy fluxes (Pytharoulis, 2018), which can influence the track and intensification of the medicanes when they occur (Tous et al., 2013b). Studies suggest that uniform changes in SST of more than 2ºC are responsible for the tropical-like cyclones (TLC) and where they are colder, the TLCs either do not form or are delayed in the development (Miglietta et al., 2011; Pytharoulis, 2018).

Remote sensing data for SST was obtained from the Copernicus Marine Environment Monitoring Service (CMEMS) product, SST EUR SST L3C NRT OBSERVATIONS from which L3 VIIRS NPP monosensor image satellite was taken (Buongiorno Nardelli et al., 2013). This dataset was already bias-corrected using METOP B as the reference sensor for the correction method. The spatial grid resolution was 0.02º X 0.02º, with a daily temporal resolution. The product manual is found at: (http://marine.copernicus.eu/documents/PUM/CMEMS-SST-PUM-010-009-031.pdf) and quality information at (http://marine.copernicus.eu/documents/QUID/CMEMS-SST-QUID-010-009-b.pdf).

The daily average of SST from the data was subset to a time range from 1st June 2020 to 31st December 2020, with one missing day it gave 213 images. This kept the event to be studied within a central time range. For the spatial dimensions, a large area which includes the study area was taken from longitude 10º to 28ºE, and latitude 32ºN to 42ºN. In all there were 901×501 pixels per day. In addition, six-hourly NRT L4 wind data used was also obtained from Copernicus Monitoring Environment Marine Service (CMEMS).

2.2.2 *Reanalysis and Model Data*

The mean sea level pressure is the average of the atmospheric pressure at sea level. The data for the pressure was taken from ERA5 reanalysis of hourly data from 1979 to date (Hersbach et al., 2020). The spatial resolution for this dataset was 0.25º × 0.25º while the temporal scale was hourly. This gave a grid scale of 57 × 41.

With the same dataset, 2-metre air temperature matching the same spatial and temporal resolutions were taken. Wind variables (eastward and northward components) were also obtained from the ERA5 reanalysis dataset, (Hersbach et al., 2020).

To calculate and evaluate the heat fluxes, the forecast albedo, surface net thermal radiation, surface net solar radiation as well as surface latent heat flux and surface sensible heat flux data were obtained from ERA5 Reanalysis dataset (Hersbach et al., 2020).

2.2.3 *Oceanographic in-situ data*

The temperature (SST) and salinity profiles were studied, in addition to the mixed layer depth (MLD). In-situ data was used for validation of the reconstructed data and to study the effect of the Medicane within the water column. For this purpose, Argo data profiles were obtained from: https://map.emodnet-physics.eu. Argo profiles data are updated every five days. Profiles were taken from June to December 2020 and between longitude 32ºN to 42ºN, latitude 14ºE to 28ºE.

Table 2. Profiles available during the period of the medicane and their positions.

Location represented	WMO	Number of Profiles	Distance from the medicane
A	6902870	3	267 km
	6901772	2	209 km
B	3901976	3	281 km
	6902875	3	69 km
	6903247	4	299 km
	6902872	3	343 km
C	6902913	3	300 km

2.2.4 *Meteorological in-situ data*

Further data from land-based stations were obtained for examination from the automated weather stations of the National Observatory of Athens Automatic Network (NOAAN) network in Greece (Lagouvardos et al., 2017). These data were for accumulated rainfall, temperature, and winds at five coastal stations of Zakynthos, Ithaki, Filiatra, Pylos and

Lefkada (shown in Fig. 1). These stations are operated by the Institute for Environmental Research and Sustainable Development (IERSD) of the National Observatory of Athens (NOA) (https://meteosearch.meteo.gr/stationInfo.asp).

2.3 Data Analysis

2.3.1 *Reconstruction of Missing Data*

Satellite images measuring in the infrared part of the electromagnetic spectrum usually have pixels with missing data due to aerosols, cloud contamination, or any fault which could affect to collection of images. This remote sensing data for SST was found to contain missing data in which cloud covers were responsible for the lack of images or coverage on some days and in some pixels. There was data missing both on spatial and temporal levels. To this end, the interpolation of the missing data was implemented using DINEOF (Data Interpolation Empirical Orthogonal Functions).

For the SST, first a reconstruction was done to fill the gappy satellite images. DINEOF (Alvera-Azcárate et al., 2005; Beckers & Rixen, 2003) is a method for data interpolation using empirical orthogonal functions. Firstly, from the 213 images collected, the percentage of missing data for each image was calculated to identify pixels that had their data missing more than 95% of the time and so are deemed to contain too few data for the reconstruction purposes. After this step, 207 images out of 213 were retained. Next, pixels that had more than 95% of missing data missing in time were considered to be land points and masked. Then cross-validation points using real cloud cover was created ensuring that the percentage of cloud cover was enough to simulate the cloud coverage in the actual images by adding missing data in the form of clouds, extracted from cloudy images to images with a small percentage of missing data.

We can perform the Single Value Decomposition for the EOFs of the matrix using the following equation:

$$X = USV^T \quad (1)$$

where X is the complete $m \times n$ matrix, U the spatial EOF having its own dimensions of $m \times r$, and V the temporal EOFs with dimension $n \times r$ and the singular values S, which has

dimensions $r \times r$. The rank of the matrix is generally designated by r where $r = min(m,n)$ if all the possible EOFs are retained. However when a truncated EOF is used as in this case, $r \ll min(m,n)$.

On each k, *an* EOF decomposition of the matrix is first done with the first k EOFs in order to obtain the first estimate of the eigenvalues and eigenvectors. Then the elements $X_{i,j}$ that correspond to the flagged missing data is replaced by the value obtained with the EOF series, thus:

$$X_{i,j} = \sum_{p=1}^{k} \rho_p \left(u_p\right)_i \left(v_p^T\right)_j \tag{2}$$

With the improved value obtained with equation 4 for the missing values, U and V are recalculated. This is repeated until convergence. Each time convergence is reached, the number of computed EOFs is increased from $k = 1,...,k_{max}$ giving $k_{\max}$ estimates for the missing data reconstructed with each EOF. Then the best estimate is selected by cross-validation.

Using cross-validation which is done using the cloud data that had been initially set aside from the valid data the optimal number of EOFs is calculated from the series of k_{max} EOFs. The optimal number of EOFs is the one that minimises the error between the data selected for cross-validation and the values obtained at those points by the reconstruction. Finally with the optimal number of EOFs N, the process is repeated but including the data that had been set aside and using only the optimal number of EOFs that was calculated. Now the final value for the missing data is computed. For this reconstruction, a total of 438627 points were set aside for cross-validation.

Based on the same idea aforementioned, a multivariate reconstruction was also carried out on cloud-contaminated satellite images. Various combinations of related variables can give a more robust calculation of the missing field (Alvera-Azcárate et al., 2007) but this is dependent on the amount of missing data in the different fields. For this multivariate reconstruction, SST was combined with lagged winds.

In terms of cost, DINEOF is based on the Lanczos method which is more efficient when dealing with large $m \times n$ matrices (Alvera-Azcárate et al., 2005; Beckers & Rixen, 2003) since it computes only the *k* largest singular values for the SVD rather than all the singular values.

2.3.2 *Validation of the reconstruction*

Having performed the reconstruction of the missing data using DINEOF, it was necessary to validate the reconstruction before performing further analysis. For this purpose, the in-situ oceanographic temperature data was used. The satellite data was linearly interpolated into the position of the in-situ data using the Argo time step that was closest to the time of the satellite pass. The root mean square error (RMSE) and the bias between the reconstructed data and the in-situ temperature data from the Argo profiles were calculated with following formulae:

$$RMSErrors = \sqrt{\frac{\sum \left(y_{fi} - y_{oi}\right)^2}{n}} \tag{3}$$

For the purpose of computing the correlations, averages were computed on the data sets. To normalize the data sets to each other before computing correlations, the hourly data sets were averaged to daily mean values, and then correlations were calculated between the atmospheric variables.

2.3.3 *Calculation of anomalies*

The anomalies were calculated based on climatology of 1982–2011 using the climatological data from ERA5 for mean sea level pressure, winds, and air temperature. The SST anomaly was calculated from 1982–2011 climatology using NOAA High Resolution SST data provided by the NOAA/OAR/ESRL PSL, (Reynolds et al., 2007).

2.3.4 *Heat Flux*

The ocean surface heat budget Qt can be computed as the downward solar radiation flux QS minus the net longwave radiation flux Qb minus the sensible heat flux Qh and

the latent heat flux Qe where the fluxes Qb , Qh and Qe are positive for energy gained by the atmosphere (Castellari et al., 1998).

2.3.5 *Relative Humidity*

The moisture content was estimated by relative humidity (RH). The following formula was used to calculate the relative humidity:

$$U = \frac{100 \exp\left[1.8096 + \left(\frac{17.2694 T_d}{237.3 + T_d}\right)\right]}{\exp\left[1.8096 + \left(\frac{17.2694 T}{237.3 + T}\right)\right]}$$

where U = Relative Humidity (%),
T = Dry Bulb Temperature (°C),
T_d = Dew Point Temperature (°C)

2.3.6 *Mixed Layer Depth*

The mixed layer depth (MLD) was determined using the Isothermal Layer Depth as the first depth where the temperature value is ±0.2°C with respect to the value at 10 m (Montégut et al., 2004).

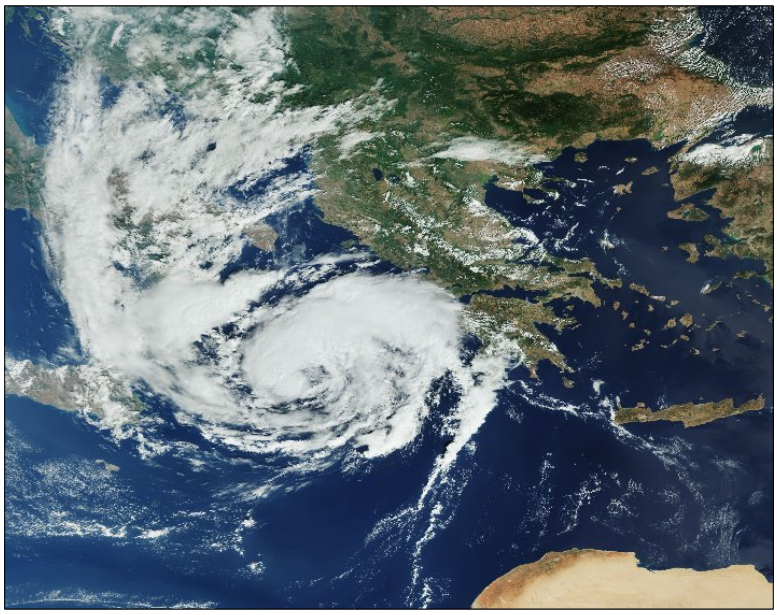

Figure 2. Medicane Ianos as seen by Copernicus Sentinel-3 mission on 17 September at 10:48 CEST. Credit: Copernicus Sentinel data (2020), processed by ESA, CC BY-SA 3.0 IGO.

3. Results

3.1 The SST (DINEOF reconstruction) Results

By means of DINEOF, the cloud-free SST reconstruction was done using both mono- and multi-variate techniques. For the monovariate reconstruction, 35 EOFs were retained, while 23 were used for the multivariate reconstruction. The mean of the reconstructed data was both lower at 23.39 than the mean of the original data prepared for the reconstruction at 24.14. The standard deviation of both reconstructions was 3.2 compared to 2.97 for the original data. A qualitative analysis showed both results to be similar. However, both reconstructions were validated with the in-situ data from 363 profiles selected between June 01, 2020, and December 31, 2020.

Table 3. Results and statistics of reconstruction

	Original L3 SST DATA	MONOVARIATE	MULTIVARIATE
RMSE (°C)	0.424	0.386	0.390
Bias (°C)	-0.157	0.121	0.123
Correlation	0.987	0.992	0.992
Size of the matrix used in DINEOF		320995 x 207	325103 x 207
Mean (°C)	24.139	23.396	23.391
Standard deviation (°C)	2.969	3.202	3.204
Number of eigenvalues retained	-	35	23
Expected error (°C)	-	0.2567	0.0905
Number of interations made	-	9	9
Convergence achieved	-	0.9748E-03	0.9388E-03
Total time (seconds) in Lanczos process	-	10474.0579	6956.1682

3.2 The validation and choice of reconstruction

For the validation, the tests of correlation, RMSE and bias were computed between the reconstructed images and the in-situ SST data. The RMS between the original SST and the in-situ data was also obtained as 0.42°C and was used as a base reference to

compare with the reconstructions. The summary of the results of both reconstructions and validations is shown in Table 3.1.

In Figure 3, we see a selection of days from the SST L3 data compared with the monovariate and multivariate reconstructions. The SST L3 data has cloudy gaps covering parts of the Central Mediterranean Sea on the selected days. These gaps fields are filled in the monovariate and multivariate reconstructions to provide complete SST fields. The uni- and multivariate fields on 13/09/2020 from both reconstructions do not show any significant differences though the multivariate SST displays cooler temperatures in the south-west.

In the image of 17/09/2020 there is a cold wake around 36°N in the monovariate reconstruction colder than that of the multivariate reconstruction. On the other hand the multivariate (MV) image shows again cooler temperatures near the coast of Greece to the north-east around 38°N. Currents are more visible in the monovariate reconstruction on this day than in the multivariate reconstruction within the Central Mediterranean.

Lastly, in the images of 20/09/2020, the L3 cloudy data shows bits of a strong cooling in the Ionian Sea which is fully reconstructed in both mono- and multivariate images. The quality is similar but there is in addition a stronger cooling in the MV reconstruction near 38°N than in the monovariate image. In general, the MV reconstruction with wind fields showed a cooler reconstruction on average compared to the monovariate reconstruction with only SST fields, except for the image on 17/09/2020 where it smoothed out the colder temperatures around 36°N. Both cloud-free images show that the absolute values of temperature are always higher in the southern part of the Central Mediterranean compared to the Ionian Sea.

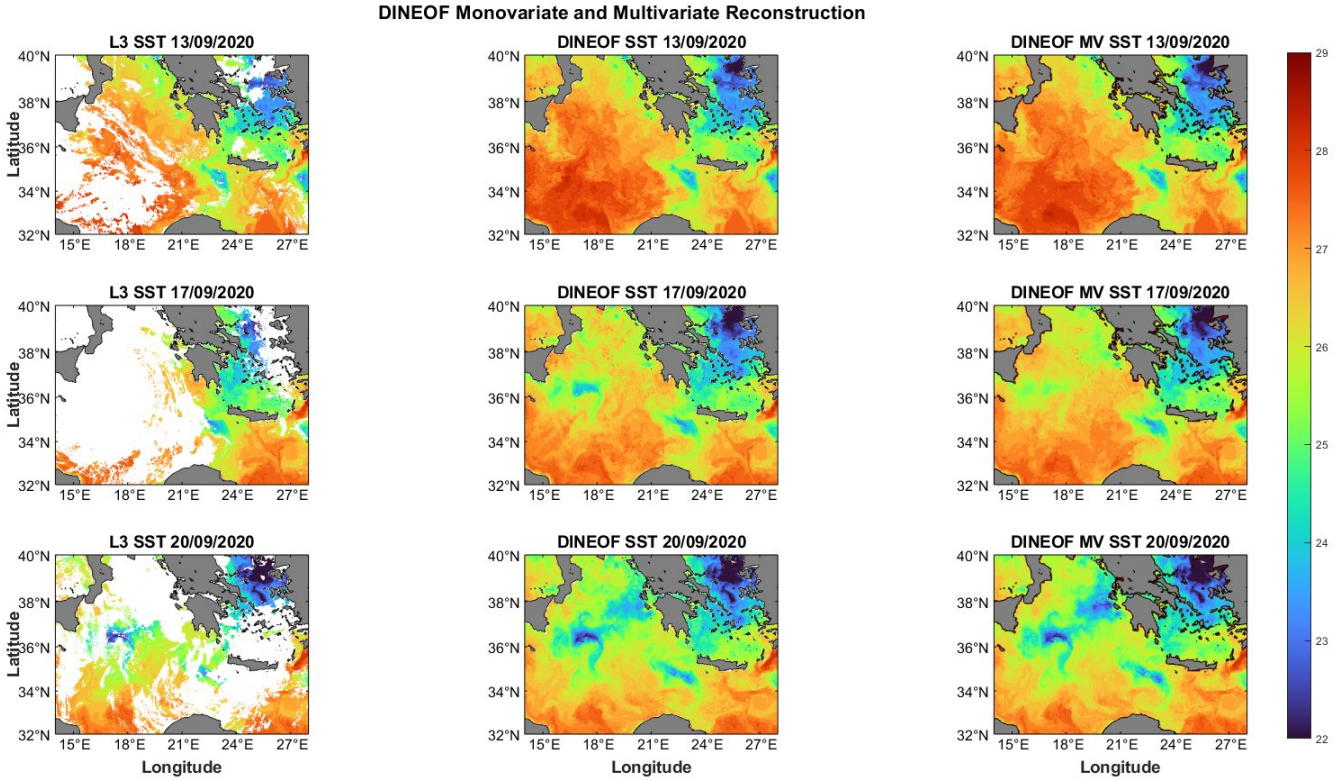

Figure 3. SST field showing a.) cloudy L3 data, b.) monovariate reconstruction and c.) multivariate reconstuction using SST + winds.

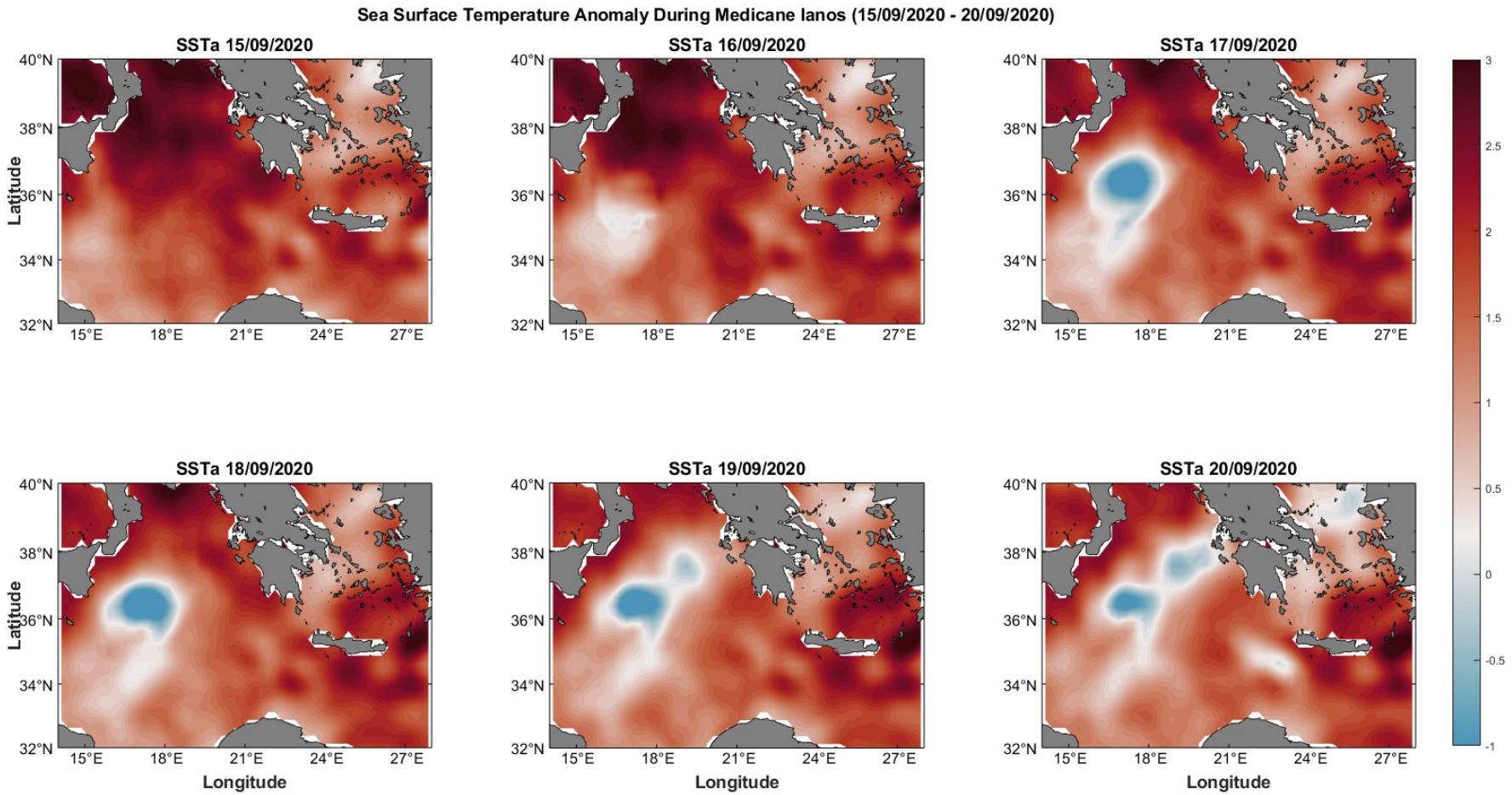
Sea Surface Temperature Anomaly During Medicane Ianos (15/09/2020 - 20/09/2020)
SSTa 15/09/2020
SSTa 16/09/2020
SSTa 17/09/2020
SSTa 18/09/2020
SSTa 19/09/2020
SSTa 20/09/2020
Latitude
Longitude
40°N
38°N
36°N
34°N
32°N
15°E
18°E
21°E
24°E
27°E
3
2.5
2
1.5
1
0.5
0
-0.5
-1

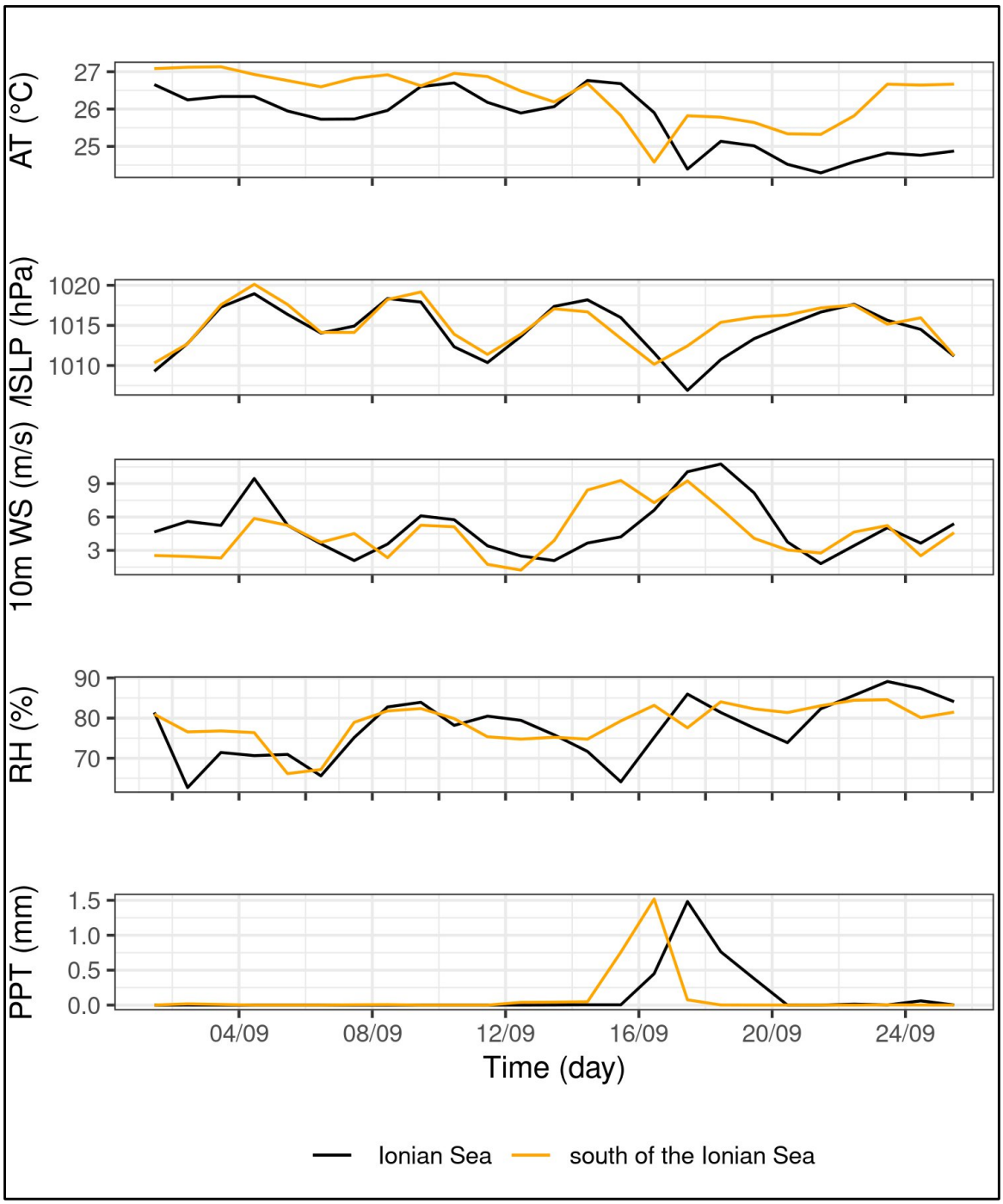

Figure 6. Timeseries of air temperature, MSLP, wind, relative humidity, and precipitation over the Central Mediterranean Sea.

The Average of Sea Surface Temperature and Atmospheric Variables During Medicane Ianos (15/09/2020 - 20/09/2020)

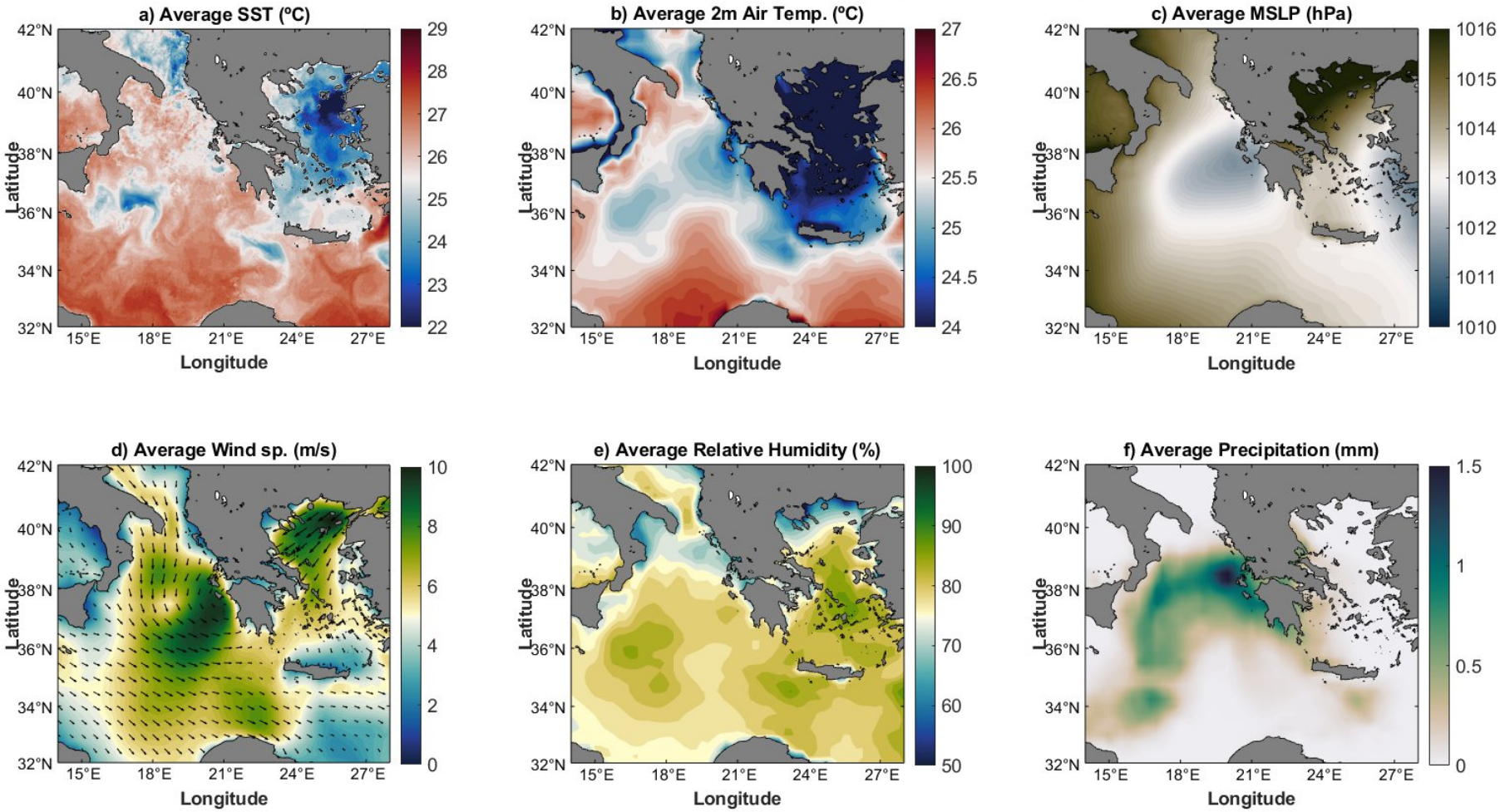

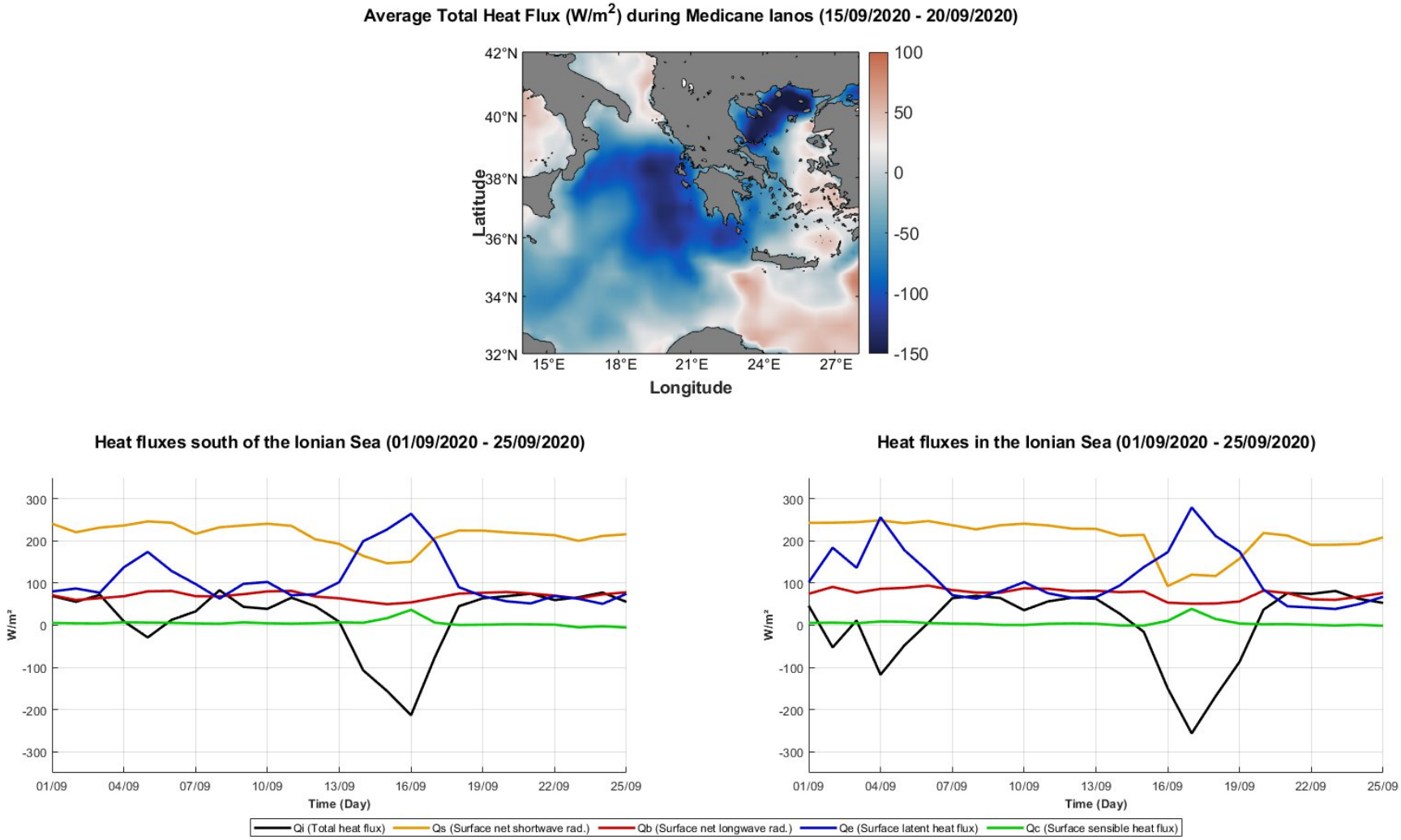

Figure 8. Heat fluxes and budget in the Central Mediterranean

3.3 Atmospheric variables and air-sea interactions during the Medicane

The daily spatial average over the south of the Ionian Sea and within the Ionian Sea was calculated from hourly data for air temperature, mean sea level pressure, wind speed, relative humidity and precipitation (Figure 6). The average over the period from 15th–20th September was calculated at each grid point to obtain the temporal average shown in Figure 7. The results are presented as follows:

Air temperature

The air temperature in the south of the Central Mediterranean was between 26.5–27°C up to the 12th of September when it began to drop and remained slightly at ~26°C for 13th–14th of September. After a brief rise, it dropped sharply by ~2°C by 17th September, remaining below 26°C until around the 23rd September (Figure 6).

For the Ionian Sea, the air temperature was ~1°C less around the 12th of September, and rose by 0.8°C between the 14–16th September before it dropped to about 24.5°C around the 17th of September and rose only slightly by about 0.5°C and remained below 25°C up to 24th of September.

The average spatial distribution of the atmospheric variables showed that between 15th–20th of September, there was cooler air temperatures of <25°C in the Ionian sea and extending along the entire west coast of Greece (Figure 7b).

Mean Sea Level Pressure

The mean sea level pressure (MSLP) in the south rose from ~1012 hPa to ~1017 hPa between 12th–14th September before it dropped to a minimum of 1010 hPa by the 16th of September, followed by a gradual return to earlier levels of ~1015 hPa. In the Ionian Sea, the MSLP average showed a deeper drop from ~1017 hPa to <1008 hPa around 17 September. The MSLP in the Ionian sea reached lower levels compared to the south of the Ionian. The lowest average MSLP was reached in the Ionian sea particularly near the coast of Greece (Figure 7c).

Wind Speed

Wind speed patterns in the south of the Central Mediterranean showed a drop in wind speed to ~3 m/s around the 12th of September (Figure 6c). The wind speed rose afterwards by up to 6 m/s around the 15th and 17th of September. In the Ionian Sea, the wind speeds increased gradually from the 13th of September up to the 18th of September when it went up to about 10.5 m/s, in the same period corresponding to the drop in MSLP. The qualitative assessment of the wind field showed that maximum winds were also found in the Ionian sea, with low wind shear outside the range of the storm towards Sicily in the west. The average wind speed calculated from the ERA5 dataset over the Ionian Sea was above 10 m/s with anticlockwise cyclonic movement around the low pressure centre of the storm (Figure 7c)..

The wind measurements obtained from weather stations in west coast of Greece where Ianos made landfall (https://meteosearch.meteo.gr/stationInfo.asp) showed similar readings. Between 17–18 September 2020 the recorded average wind speed at Filiatra was 8km/h while the highest wind gusts was 38.6km/h. Similarly wind speeds were 13 km/h (highest values at 67.6 km/h) at Zakynthos, 12 km/h (high of 66 km/hr) at Pylos, 17.5 km/h (high values of 90 km/hr) at Ithaca and 20 km/h (high values at 83km/h) at Lefkada.

Relative Humidity

Moisture content is one of the conditions for the beginning of a tropical cyclone (Anthes, 1974). The moisture content was measured by the relative humidity (RH) calculated as a function of the air temperature and dew point temperature. In the south (Figure 6d)., the RH was about 75% pre-storm, and then increased to ~82% during the storm, where it remained up till 24th September. In the Ionian Sea, the RH was higher at ~80% by 12th September, dropped sharply to ~65% and rose to 85% during the storm between 17th and 18th September. It remained above 75% on average till the end of the storm. This drop was likely as a result conversion from potential to kinetic energy by the air masses (Wallace & Hobbs, 2006; Anthes, 1974).

Average RH (Figure 7c) for the entire period between September 14–20 was ~80% with the maximum values around 18°E off the east of Sicily and also around 24°E. The first location corresponds to the position where the storm intensified with maximum average decrease in SST and SST anomaly. The second location (24°E) corresponds to the end of life of the medicane. The high relative humidity at the start of the medicane confirmed that it was a key part of cyclone formation.

Precipitation

Precipitation (Figure 6e) was not almost non-existent before the storm in both study areas. It went up to 1.5 mm hourly between 14th and 17th of September in the south, and 16th–18th September in the Ionian Sea. While precipitation returned to pre-storm levels by 17th September in the south, the Ionian Sea had precipitation up to 20th of September. A spatial qualitative analysis (Figure 7e) shows that there was a gradual increase of precipitation with the progress of the storm and it reached its maximum average around the coast of Greece when the storm made landfall. At the coastal areas, accumulated rainfall was 93 mm at Filiatra, 59.2 mm at Pylos, 227.4 mm at Ithaki and 110 mm of rainfall at Lefkada stations for the 17th and 18th of September.

A test of correlation and cross-correlation was done to assess the nature of the interaction between SST and the atmospheric variables using daily average over the domain for each variable. The outcome showed that SST was strongly correlated to only air temperature ($r = 0.841$) and SST led the change in air temperature with a lag of 1. In the test of cross-correlation with pressure, the SST lagged behind pressure by 2 days. Comparing between SST and the wind, showed a negative correlation between both variables. In addition, the wind led SST changes by a lag of 2. Furthermore, SST also lagged behind precipitation by 2. This finding suggests that part of the reason for the changes in the SST was due to the changes in the winds and the precipitations.

Heat Flux

The passage of Medicane Ianos led to an observable change in the heat fluxes in both parts of the Central Mediterranean. In location A (the south), the average surface latent heat flux rose from around 60 W/m² before the storm to about 250 W/m² on the 16th of

September (Figure 8), while the total heat flux in the same location dropped from about 50 W/m² to around –200 W/m² in the same period. At the same time the surface net shortwave radiation decreased by about 60–80 W/m². The fluxes returned to pre-storm levels around the 19th of September.

In the Ionian sea, the maximum total heat flux was about –250W/m² occurring around the 17th–18th of September. The surface latent heat flux to the atmosphere was similar to that in location A, but the net shortwave radiation dropped further by about 50W/m² in the Ionian Sea. While this change in heat flux began around the 13th and intensified around the 15th of September, it is only around the 21st of September that it returned to pre-medicane levels. The qualitative assessment showed that during the medicane maximum average total heat flux to the atmosphere was within the Ionian Sea and closer to the Greek coasts than in the south.

Salinity and Temperature

In this study profiles used for the validation of SST were subset to the period of the medicane. Three groups were selected according to location as follows: group A was in the south of the Ionian Sea, group B was in the central Ionian Sea, and group C was west of the Island of Crete. The path of the medicane went first by A, then B and lastly C. Of the three, C is removed from the active medicane as it only arrives there near the end of the life cycle. The salinity and temperature profiles are shown up to depth of 120 meters.

In Figure 9, the profiles at the south of the Ionian sea are reproduced showing the salinity and temperature up to a depth of 125 m below the surface. In location A the last measure of salinity before the storm was about 38.25 psu. During the medicane, it dropped to about 38.15 psu. After the medicane, the measured salinity was about 37.9 psu at the surface. This suggested a drop in salinity of around 0.35 psu. The temperature profile also registered a similar change. Temperature values dropped to around 26.8°C from about 28.5°C pre-storm, and remained at ~26.75°C after the storm. In the Ionian sea (location B), the salinity increased from 38.8 psu before the storm, to about 38.95 psu. However this value dropped to about 38.7 psu after the medicane. For the temperature profile, it was observed that the drop was first from 27.5°C to ~26.8°C and then dropped further to

~23.7°C representing an overall drop of ~3.8°C. This was indicative of the upwelling of colder and more saline waters to the surface.

The Argo profiles at location C is used as reference to compare the effect of the medicane since this profile was the last from the path of the active Medicane Ianos. The only significant change is observed in the salinity profile at the surface which decreased from ~39.55 psu to about 39.45 psu during the medicane and remained at the same range after Medicane Ianos had passed while below the mixed layer, the salinity increased from about 38.7 psu to 39.0 psu, a change of ~0.3 psu.

In the temperature profile, there is no significant change in the temperature before, during or after the medicane as the temperature drops from about 26.5°C (pre-storm), to ~ 25.9°C post-storm.

Mixed Layer Depth

In the various parts of the Mediterranean Sea, the mixed layer depth has a seasonal variability. In summer around September, the MLD in the Ionian sea is about 15–30 m D'Ortenzio et al., (2005). This is visible from the Argo profiles in A, B and C. Pre-medicane, each of them is at ~25 m. During the medicane the mixed layer depth (MLD) at location A increased by about 20 m (Figure 3.7A) and decreased slightly by about 6 m post-storm. At location B (in the Ionian Sea) the MLD increased by about 10m during the medicane and a further ~3m post-medicane. With the profile at the reference location (C), there is no observed change in the MLD.

Chlorophyll-a concentration

The daily average of chlorophyll-a was calculated for the time series. The daily distribution at each grid point was also extracted for 15–20th September, 2020. This showed the impact of the medicane in the upwelling of nutrients to the surface of the ocean. The highest values of chlorophyll-a were just south of the Ionian Sea around latitude 36°N (Figure 3.10) where the first sign of cooling had appeared on 17th of September. The maximum Chl-a values during the medicane was ~0.4 mg/m³ in the Ionian Sea with average of 0.08 mg/m³ up from 0.035mg/m³ before the medicane, whereas in the south the maximum values of Chl-a was about 0.23 mg/m³ while the average was about 0.1

mg/m³ from pre-storm values of 0.04 mg/m³. The spatial distribution of the Chl-a also shows that most of it was due to the upwelling on 17th of September.

Salinity / Temperature Profiles

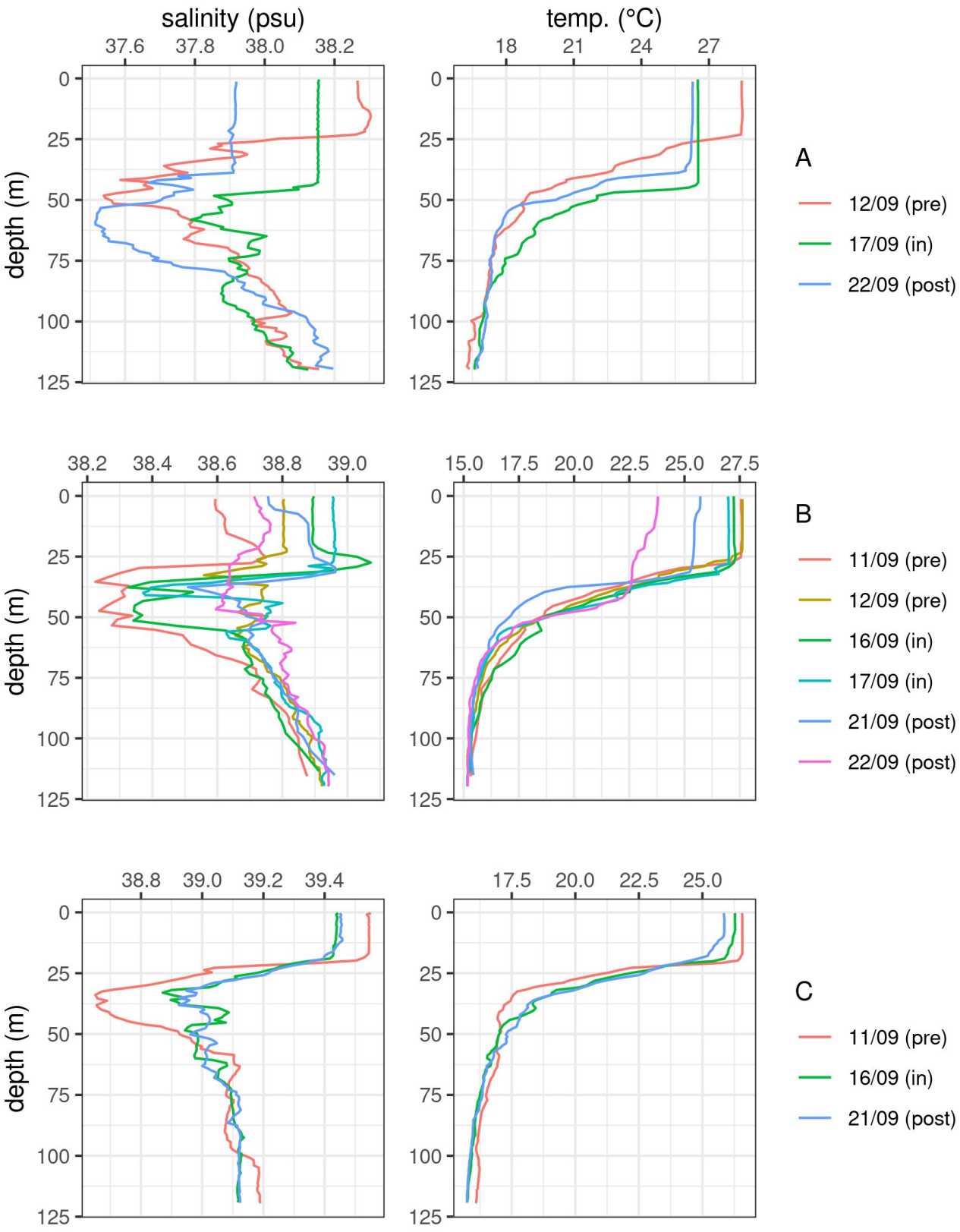

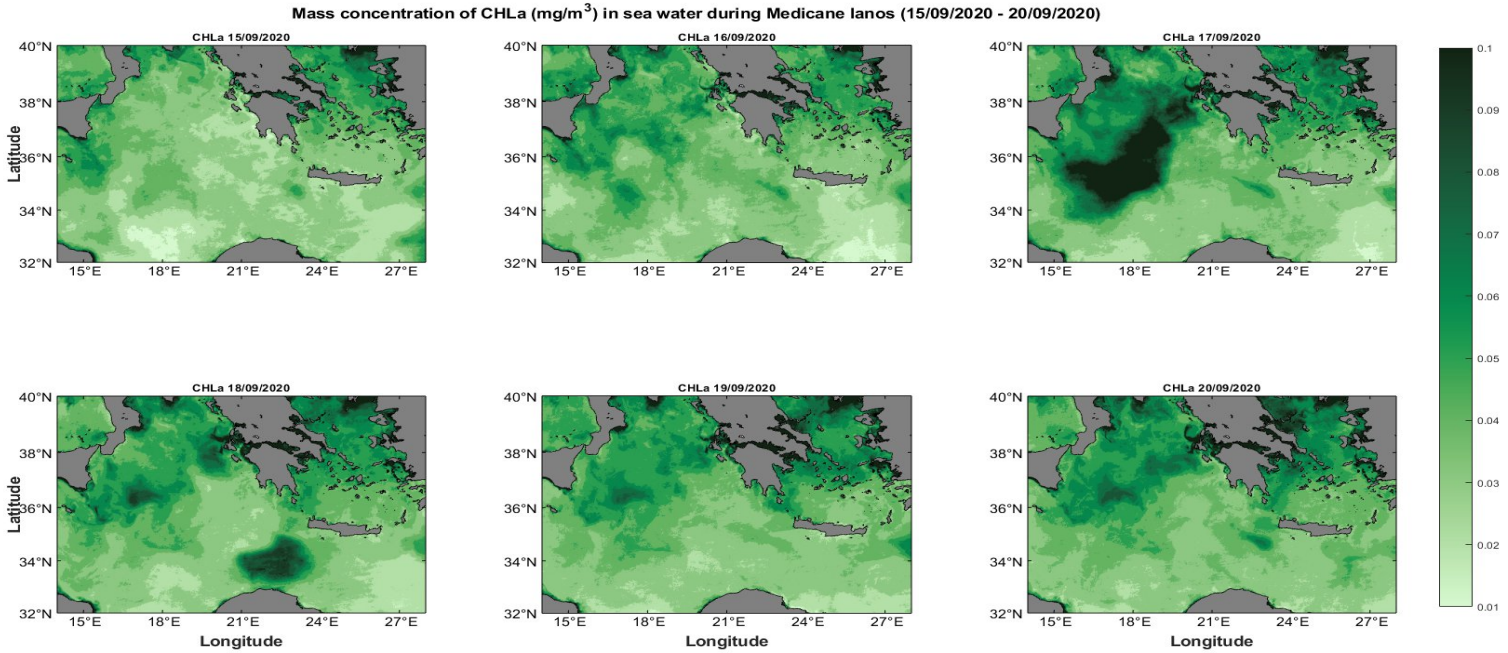

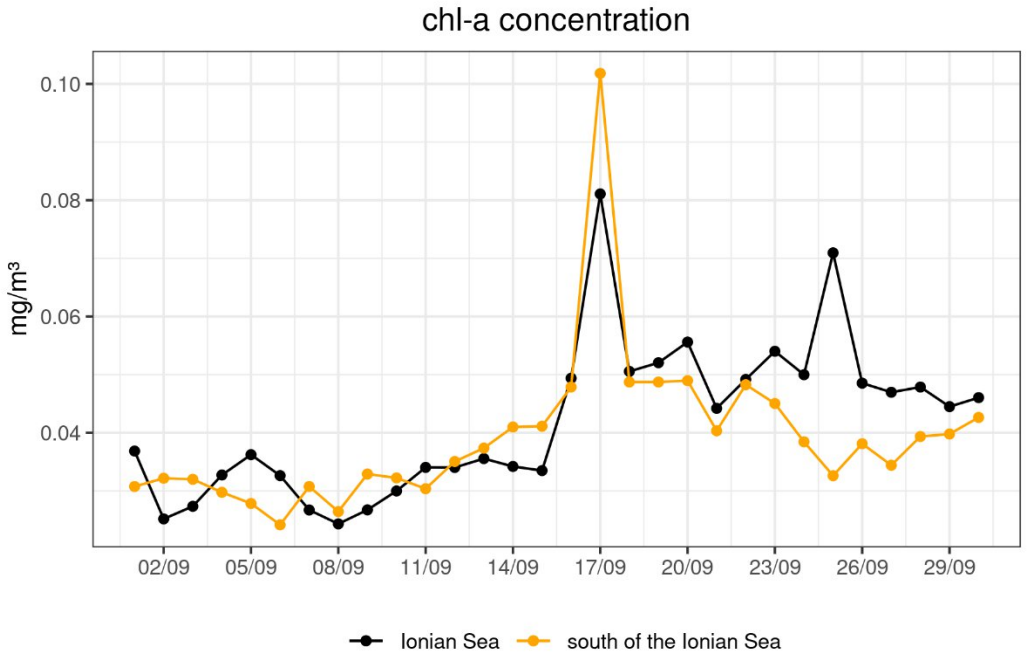

Figure 10. Chlorophyll concentration from15 to 20 September 2020

4. Discussion

We can attempt to trace the life cycle of the storm as follows. It began in the Gulf of Sidra on 14th of September when high SST and evaporation led to a change in the atmospheric pressure. Four components are required in the formation of a cyclone: pressure, winds, temperature and moisture content (Anthes, 1974).

The moisture content in the atmosphere and the drop in the pressure in turn led to the gradual increase in the wind fields. This change in wind field following the MSLP is visible from the timeseries (Figure 6) as the wind field increased following a drop in the MSLP. As the air temperature was influenced by the changes in SST, pressure and winds, it was observed to rise sharply before a sudden drop (Castellari et al., 1998).

The cold front, with warm air on the east and cold air on the west, made a northeastern movement into the Ionian sea. The presence of rising warm air led to a conversion of potential energy to kinetic energy associated to the meridional wind component inducing storm intensification. The storm was able to maintain the vortex due to the weak vertical wind shear. Stronger winds were present to the right of the storm as a result of the imposition between the forward movement of the storm and the cyclonic circulation around it.

As it entered the Ionian Sea where the SST anomaly was higher than the usual, the core began to warm owing to the heating of the inflow air by the air-sea fluxes. The warm-core of tropical cyclone enabled it to draw energy from the fluxes at the air-sea interface. Upper tropospheric divergence caused the sea level pressure to drop until it got to about 988 hPa, and led to increased wind speed which rotate as a result of the Coriolis force. The rapid decrease in pressure is due to subsidence of upper tropospheric air with high potential temperature which is necessary to maintain the low surface pressure in the eye of the storm. This central core of subsidence is supported by the high temperatures and the absence of clouds (Anthes, 1974). The rapid replacement of the rising warm air by the cold tropospheric air leads to increased cyclonic wind speeds. At the same time, the increase in surface winds led to an increase in the latent and sensible heat fluxes from the ocean surface inducing stronger heating in the storm interior which led to further drop

in the surface pressure. The convergence of cold and warm fronts then pushed moisture into the air creating precipitation and clouds that form the cloud wall of the storm.

By the time the 'eye' of the cyclone was clearly formed the medicane had most of the characteristics of a tropical cyclone with the only exception that it was restricted to a smaller area. From the edge of the eye wall to the centre, there was a drop in the horizontal winds and the subsidence of air masses to the centre ensured that the eye remained relatively dry. With the intense winds gusts of up to 36 m/s, Medicane Ianos made landfall at Greece by the 18th of September. The end of the intensification phase in the life cycle of medicane Ianos was linked to change from baroclinic to barotropic waves (Wallace and Hobbs, 2006). The high wind speed of Medicane Ianos which was up to 33 ms^{1} (118km/h) qualified it to be ranked as a Category 1 Hurricane according to the Saffir-Simpson Scale (Saffir, 1973;Simpson, 1974). The high precipitation near the coasts was linked to cases of flooding, landslides and heavy rainfall across central Greece, and not only at the islands (Zekkos et al., 2020).

Owing to the landfall Ianos lost the heat fluxes that were required to sustain the eye wall and maintain an intense storm. The remnant of Medicane Ianos travelled south in the direction of the Island of Crete and the Levantine Basin where it dissipated.

The signal of the reduced salinity in Location A could be attributed to the high rainfall as the salinity before the medicane (38.2 psu) was the minimum signal associated to the AW (Kassis & Varlas, 2020) before it dropped to 37.9 psu after the medicane. The profile in location A was closer to the MAW while profile group B showed signals of the Levantine Intermediate Water (LIW) (Millot & Taupier-Letage, 2005; Robinson et al., 2001). In addition to the changes at the surface, there is evidence of the movement of water masses below the surface resulting to horizontal advection. This is recognised from the increase in salinity at depths 25–50 m. Location C was influenced by the Levantine Surface Water (LSW) as evident from the high salinity and lower temperature values of the profile.The salinity The changes in the salinity and temperature profiles agree with (Kassis & Varlas, 2021).

Zhang and McPhaden (1995) observed that at low SST, latent heat flux increased with SST, while at high SST the latent heat decreased with increasing SST. This interesting relationship is influenced by the presence of winds and humidity. The humidity difference determines the latent heat flux at low SST, while at high SST the latent heat flux is influenced by winds. During the passage of Medicane Ianos, the surface latent heat flux released to the atmosphere was large (~ 250 W/m²). It has already been remarked the presence of high winds during the medicane. There was a drop in shortwave radiation as a result of the presence of the clouds formed during the medicane. This would have affected the energy budget at the sea surface but the surface latent heat flux is the second largest component after the shortwave radiation (Zhang & McPhaden, 1995). The presence of high SST and low winds before the medicane meant that the latent heat flux would have been low before the medicane, and this is visible in the timeseries (Figure). As a result of the medicane, the increase in winds not only led to the increase in the surface latent heat flux but also contributed to the decrease in SST. This agrees with previous studies on the relationship between latent heat flux and SST (Kumar et al., 2017; Zhang & McPhaden, 1995).

The Coriolis force acting on the spinning water induces a radial outflow leading to Ekman pumping and upwelling (Wallace &Hobbs, 2006) which was observed near the centre of the cyclone especially on the 17th of September. This was confirmed by the signal increase of chlorophyll-a concentration after the medicane. Even though it was short-lived, this showed that medicanes, like tropical cyclones, can also lead to chlorophyll bloom (Chen & Tang, 2012; Liu et al., 2020). Mesoscale eddies are found here in addition to the MAW circulation and the Ionian Anticyclones (IA) (Robinson et al., 2001, Mikhinini et al., 2014). The Chl-a was upwelled to the surface due to the vertical mixing that brought up nutrient-rich waters from below the mixed layer and the thermocline (Yin et al., 2007). Liu et al.,(2020) also showed that the upwelling of Chl-a was linked to SST cooling and the high winds.

Medicane Ianos intensified on17th of September, with the lowest surface pressure of about 995 hPa. The SST cooling associated to this intensification was also ~–3°C. The Argo float at Location A also showed the deepening of the MLD by up to 25 m. This would

explain that after Medicane Ianos passed, wind-induced vertical mixing propagated colder waters from the subsurface which not only induced Chl-a upwelling but also contributed to the cooling of SST. (Kassis & Varlas, 2021; Sriver & Huber, 2007).

5. Conclusion

The Medicane Ianos began as a tropical low pressure cyclone in the Gulf of Sidra. Then the storm moved into the Ionian Sea towards the region of high SST anomalies of up to 3°C compared to the climatological average (1982–2011) which contributed to the intensification of the storm into a tropical-like cyclone (medicane) despite the lower SST (<26°C) (Tous & Romero, 2013; Varlas et al., 2020).

Mono- and multivariate reconstructions of L3 satellite data was carried out using DINEOF. The reconstructed L4 data was able to show the passage of the medicane across the Ionian sea. Combined with other variables, the effect of the medicane within the ocean layer was also studied. During the lifetime of medicane Ianos, the SST dropped in the wake of the medicane by ~3–4°C. This signal was observed both with the satellite data and the in-situ data obtained from the Argo profiles.

Drop in pressure and increased winds resulted to air-sea interactions that affected the ocean heat budget. Surface latent heat flux to the atmosphere was high. It was not possible to see how the surface fluxes may have influenced the medicane trajectory but the relation to the intensification as proposed by Tous et. al.,(2013) was visible. Moreso the feedback between the medicane and the heat fluxes was also observed. Due to the cyclonic movements, average total heat loss to the atmosphere was about –200W/m² over the Central Mediterranean sea during the lifetime of Ianos.

It was also observed that the medicane led to an increase of the mixed layer depth beyond the average seasonal MLD by about 12–15 m, and changes in salinity by between ±0.1 – 0.35 psu and change in the potential temperature by 2–4°C within the surface layer of the ocean. This agrees with previous hydrographic studies on medicane effects such as Drobinski et al., (2014), Kassis & Korres, (2020) and Kassis & Varlas, (2021). In addition, upwelling was observed with the passage of the medicane, with Chl-a values up to 1.04 mg/m³ and average of 0.07 mg/m³ from 0.038mg/m³.

In all through this study it was possible to see the impact of Medicane Ianos in the Ionian Sea between 15th –20th of September, 2020. Further recommendations to this study

would be to calculate the ocean heat content with respect to the medicane, look more closely to the state of the ocean before the medicane and also examine the effect of the medicane on sea surface height.

References:

1. Alvera-Azcárate, A., Barth, A., Beckers, J.-M., & Weisberg, R. H. (2007). Multivariate reconstruction of missing data in sea surface temperature, chlorophyll, and wind satellite fields. *Journal of Geophysical Research*, *112*(C3), C03008. https://doi.org/10.1029/2006JC003660
2. Alvera-Azcárate, A., Barth, A., Rixen, M., & Beckers, J. M. (2005). Reconstruction of incomplete oceanographic data sets using empirical orthogonal functions: Application to the Adriatic Sea surface temperature. *Ocean Modelling*, *9*(4), 325–346. https://doi.org/10.1016/j.ocemod.2004.08.001
3. Anthes, R. A. (1974). The dynamics and energetics of mature tropical cyclones. *Reviews of Geophysics*, *12*(3), 495. https://doi.org/10.1029/RG012i003p00495
4. Beckers, J. M., & Rixen, M. (2003). EOF Calculations and Data Filling from Incomplete Oceanographic Datasets. *JOURNAL OF ATMOSPHERIC AND OCEANIC TECHNOLOGY*, *20*, 18.
5. Buongiorno Nardelli, B., Tronconi, C., Pisano, A., & Santoleri, R. (2013). High and Ultra-High resolution processing of satellite Sea Surface Temperature data over Southern European Seas in the framework of MyOcean project. *Remote Sensing of Environment*, *129*, 1–16. https://doi.org/10.1016/j.rse.2012.10.012
6. Castellari, S., Pinardi, N., & Leaman, K. (1998). A model study of air–sea interactions in the Mediterranean Sea. *Journal of Marine Systems*, *18*(1–3), 89–114. https://doi.org/10.1016/S0924-7963(98)90007-0
7. Cavicchia, L., von Storch, H., & Gualdi, S. (2014a). A long-term climatology of medicanes. *Climate Dynamics*, *43*(5–6), 1183–1195. https://doi.org/10.1007/s00382-013-1893-7
8. Cavicchia, L., von Storch, H., & Gualdi, S. (2014b). Mediterranean Tropical-Like Cyclones in Present and Future Climate. *Journal of Climate*, *27*(19), 7493–7501. https://doi.org/10.1175/JCLI-D-14-00339.1
9. Chen, Y., & Tang, D. (2012). Eddy-feature phytoplankton bloom induced by a tropical cyclone in the South China Sea. *International Journal of Remote Sensing*, *33*(23), 7444–7457. https://doi.org/10.1080/01431161.2012.685976
10. D'Ortenzio, F., Iudicone, D., Montegut, C. de B., Testor, P., Antoine, D., Marullo, S., Santoleri, R., & Madec, G. (2005). Seasonal variability of the mixed layer depth in the Mediterranean Sea as derived from in situ profiles. *Geophysical Research Letters*, *32*(12). https://doi.org/10.1029/2005GL022463
11. Emanuel, K. (2005). Genesis and maintenance of "Mediterranean hurricanes" *Advances in Geosciences*, *2*, 217–220. https://doi.org/10.5194/adgeo-2-217-2005
12. Gray, W.M, 1981: Recent Advances in Tropical Cyclone Research from Rawinsonde Composite Analysis. World Meteorological Organization, 407 pp.
13. Henderson-Sellers, A., Zhang, H., Berz, G., Emanuel, K., Gray, W., Landsea, C., Holland, G., Lighthill, J., Shieh, S.-L., Webster, P., & McGuffie, K. (1998). Tropical Cyclones and Global Climate Change: A Post-IPCC Assessment. *Bulletin of the*

American Meteorological Society, *79*(1), 19–38. https://doi.org/10.1175/1520-0477(1998)079<0019:TCAGCC>2.0.CO;2
14. Hersbach, H., Bell, B., Berrisford, P., Hirahara, S., Horányi, A., Muñoz-Sabater, J., Nicolas, J., Peubey, C., Radu, R., Schepers, D., Simmons, A., Soci, C., Abdalla, S., Abellan, X., Balsamo, G., Bechtold, P., Biavati, G., Bidlot, J., Bonavita, M., … Thépaut, J. (2020). The ERA5 global reanalysis. *Quarterly Journal of the Royal Meteorological Society*, *146*(730), 1999–2049. https://doi.org/10.1002/qj.3803
15. Holland G.J. Ed., 1993: The Global Guide to Tropical Cyclone Forecasting. World Meteorological Organization, 337 pp
16. Homar, V., Homar, V., Ramis, C., & Alonso, S. (2002). A deep cyclone of African origin over the Western Mediterranean: Diagnosis and numerical simulation. *Annales Geophysicae*, *20*, 93–106. https://doi.org/10.5194/angeo-20-93-2002
17. Horvath, K., Fita, L., Romero, R., & Ivan, B. (2004). *THE INFLUENCE OF OROGRAPHY DURING DEEP MEDITERRANEAN CYCLOGENESIS 11-15 NOVEMBER 2004*. 4.
18. Jacox, M. G., Alexander, M. A., Mantua, N. J., Scott, J. D., Hervieux, G., Webb, R. S., & Werner, F. E. (2016). Forcing of Multiyear Extreme Ocean Temperatures that Impacted California Current Living Marine Resources in 2016. *Bulletin of the American Meteorological Society*, *99*(1), S27–S33. https://doi.org/10.1175/BAMS-D-17-0119.1
19. Jones, T., Parrish, J. K., Peterson, W. T., Bjorkstedt, E. P., Bond, N. A., Ballance, L. T., Bowes, V., Hipfner, J. M., Burgess, H. K., Dolliver, J. E., Lindquist, K., Lindsey, J., Nevins, H. M., Robertson, R. R., Roletto, J., Wilson, L., Joyce, T., & Harvey, J. (2018). Massive Mortality of a Planktivorous Seabird in Response to a Marine Heatwave. *Geophysical Research Letters*, *45*(7), 3193–3202. https://doi.org/10.1002/2017GL076164
20. Kassis, D., & Varlas, G. (2021). Hydrographic effects of an intense “medicane” over the central-eastern Mediterranean Sea in 2018. *Dynamics of Atmospheres and Oceans*, *93*, 101185. https://doi.org/10.1016/j.dynatmoce.2020.101185
21. Kumar, B. P., Cronin, M. F., Joseph, S., Ravichandran, M., & Sureshkumar, N. (2017). Latent Heat Flux Sensitivity to Sea Surface Temperature: Regional Perspectives. *Journal of Climate*, *30*(1), 129–143. https://doi.org/10.1175/JCLI-D-16-0285.1
22. Lagouvardos, K., Kotroni, V., Bezes, A., Koletsis, I., Kopania, T., Lykoudis, S., Mazarakis, N., Papagiannaki, K., & Vougioukas, S. (2017). The automatic weather stations NOANN network of the National Observatory of Athens: Operation and database. *Geoscience Data Journal*, *4*(1), 4–16. https://doi.org/10.1002/gdj3.44
23. Link, L. E. (2010). The anatomy of a disaster, an overview of Hurricane Katrina and New Orleans. *Ocean Engineering*, *37*(1), 4–12. https://doi.org/10.1016/j.oceaneng.2009.09.002

24. Liu, Y., Tang, D., Tang, S., Morozov, E., Liang, W., & Sui, Y. (2020). A case study of Chlorophyll a response to tropical cyclone Wind Pump considering Kuroshio invasion and air-sea heat exchange. *Science of The Total Environment*, *741*, 140290. https://doi.org/10.1016/j.scitotenv.2020.140290
25. Mastrantonas, N., Herrera-Lormendez, P., Magnusson, L., Pappenberger, F., & Matschullat, J. (2021). Extreme precipitation events in the Mediterranean: Spatiotemporal characteristics and connection to large-scale atmospheric flow patterns. *International Journal of Climatology*, *41*(4), 2710–2728. https://doi.org/10.1002/joc.6985
26. McCabe, R. M., Hickey, B. M., Kudela, R. M., Lefebvre, K. A., Adams, N. G., Bill, B. D., Gulland, F. M. D., Thomson, R. E., Cochlan, W. P., & Trainer, V. L. (2016). An unprecedented coastwide toxic algal bloom linked to anomalous ocean conditions. *Geophysical Research Letters*, *43*(19). https://doi.org/10.1002/2016GL070023
27. Miglietta, M. M., & Rotunno, R. (2019). Development mechanisms for Mediterranean tropical-like cyclones (medicanes). *Quarterly Journal of the Royal Meteorological Society*, *145*(721), 1444–1460. https://doi.org/10.1002/qj.3503
28. Miglietta, M. M., Moscatello, A., Conte, D., Mannarini, G., Lacorata, G., & Rotunno, R. (2011). Numerical analysis of a Mediterranean 'hurricane' over south-eastern Italy: Sensitivity experiments to sea surface temperature. *Atmospheric Research*, *101*(1–2), 412–426. https://doi.org/10.1016/j.atmosres.2011.04.006
29. Millot, C., & Taupier-Letage, I. (2005). Circulation in the Mediterranean Sea. In A. Saliot (Ed.), *The Mediterranean Sea* (Vol. 5K, pp. 29–66). Springer Berlin Heidelberg. https://doi.org/10.1007/b107143
30. Nastos, P. T., Karavana Papadimou, K., & Matsangouras, I. T. (2018). Mediterranean tropical-like cyclones: Impacts and composite daily means and anomalies of synoptic patterns. *Atmospheric Research*, *208*, 156–166. https://doi.org/10.1016/j.atmosres.2017.10.023
31. Neumann, C. J., 1993: Global overview. Global Guide to Tropical Cyclone Forecasting, WMO/TC-No. 560, Rep. TCP-31, World Meteorological Organization, Geneva, Switzerland, 220 pp. [Available from World Meteorological Organization,
32. Neumann, C.J, Cry, G. W., Caso F. L., and Jarvinen B. R. 1985: Tropical Cyclones of the North Atlantic Ocean, 1871-1980. NOAA Special Publication, 174 pp.
33. P.O. Box 2300, 41, Avenue Giuseppe Motta, CH-1211, Geneva 2, Switzerland.]
34. Pytharoulis, I. (2018). Analysis of a Mediterranean tropical-like cyclone and its sensitivity to the sea surface temperatures. *Atmospheric Research*, *208*, 167–179. https://doi.org/10.1016/j.atmosres.2017.08.009
35. Pytharoulis, I., Craig, G., & Ballard, S. (2000). The hurricane-like Mediterranean cyclone of January 1995. *Meteorlogical Applications*, *7*(3), 261–279. https://doi.org/10.1017/S1350482700001511

36. Pytharoulis, I., Kartsios, S., Tegoulias, I., Feidas, H., Miglietta, M., Matsangouras, I., & Karacostas, T. (2018). Sensitivity of a Mediterranean Tropical-Like Cyclone to Physical Parameterizations. *Atmosphere*, *9*(11), 436. https://doi.org/10.3390/atmos9110436
37. Reynolds, R. W., Smith, T. M., Liu, C., Chelton, D. B., Casey, K. S., & Schlax, M. G. (2007). Daily High-Resolution-Blended Analyses for Sea Surface Temperature. *Journal of Climate*, *20*(22), 5473–5496. https://doi.org/10.1175/2007JCLI1824.1
38. Robinson, A. R., Leslie, W. G., Theocharis, A., & Lascaratos, A. (2001). Mediterranean Sea Circulation. In *Encyclopedia of Ocean Sciences* (pp. 1689–1705). Elsevier. https://doi.org/10.1006/rwos.2001.0376
39. Rudnick, D. L., Zaba, K. D., Todd, R. E., & Davis, R. E. (2017). A climatology of the California Current System from a network of underwater gliders. *Progress in Oceanography*, *154*, 64–106. https://doi.org/10.1016/j.pocean.2017.03.002
40. Sriver, R. L., & Huber, M. (2007). Observational evidence for an ocean heat pump induced by tropical cyclones. *Nature*, *447*(7144), 577–580. https://doi.org/10.1038/nature05785
41. Tibaldi, S., & Buzzi, A. (1983). Effects of orography on Mediterranean lee cyclogenesis and its relationship to European blocking. *Tellus A*, *35A*(4), 269–286. https://doi.org/10.1111/j.1600-0870.1983.tb00203.x
42. Tous, M., & Romero, R. (2013). Meteorological environments associated with medicane development: METEOROLOGICAL ENVIRONMENTS ASSOCIATED WITH MEDICANE DEVELOPMENT. *International Journal of Climatology*, *33*(1), 1–14. https://doi.org/10.1002/joc.3428
43. Tous, M., Romero, R., & Ramis, C. (2013a). Surface heat fluxes influence on medicane trajectories and intensification. *Atmospheric Research*, *123*, 400–411. https://doi.org/10.1016/j.atmosres.2012.05.022
44. Tous, M., Romero, R., & Ramis, C. (2013b). Surface heat fluxes influence on medicane trajectories and intensification. *Atmospheric Research*, *123*, 400–411. https://doi.org/10.1016/j.atmosres.2012.05.022
45. Trenberth, K. (2005). CLIMATE: Uncertainty in Hurricanes and Global Warming. *Science*, *308*(5729), 1753–1754. https://doi.org/10.1126/science.1112551
46. Trenberth, K. E., & Shea, D. J. (2006). Atlantic hurricanes and natural variability in 2005. *Geophysical Research Letters*, *33*(12), L12704. https://doi.org/10.1029/2006GL026894
47. Trigo, I. F., Davies, T. D., & Bigg, G. R. (1999). Objective Climatology of Cyclones in the Mediterranean Region. *Journal of Climate*, *12*(6), 1685–1696. https://doi.org/10.1175/1520-0442(1999)012<1685:OCOCIT>2.0.CO;2
48. Varlas, G., Vervatis, V., Spyrou, C., Papadopoulou, E., Papadopoulos, A., & Katsafados, P. (2020). Investigating the impact of atmosphere–wave–ocean

interactions on a Mediterranean tropical-like cyclone. *Ocean Modelling*, *153*, 101675. https://doi.org/10.1016/j.ocemod.2020.101675

49. Wang, Z. (2015). TROPICAL CYCLONES AND HURRICANES | Tropical Cyclogenesis. In *Encyclopedia of Atmospheric Sciences* (pp. 57–64). Elsevier. https://doi.org/10.1016/B978-0-12-382225-3.00506-5
50. Yin, X., Wang, Z., Liu, Y., & Xu, Y. (2007). Ocean response to Typhoon Ketsana traveling over the northwest Pacific and a numerical model approach. *Geophysical Research Letters*, *34*(21).
51. Zekkos D., Zalachoris G., Alvertos, A. E., Amatya P. M., Blunts P., Clark M., Dafis S., Farmakis I., Ganas A., Hille M., Kalimogiannis V., Karagiannidis A., Karantanellis E., Khan K., Kirshbaum D., Kourkoulis R., Kotroni V., Ktenidou O.-J., Lagouvardos K., Loli M., Makrinikas A., Marinos V., Manousakis J., Nikas K., Panousis D., Papathanassiou G., Saroglou C., Simopoulos A., Stanley T., Tsavalas A., Valkaniotis S. “The September 18-20 2020 Medicane Ianos Impact on Greece - Phase I Reconnaissance Report”. Geotechnical Extreme Events Reconnaissance Report, GEER-068, https://doi.org/10.18118/G6MT1T.
52. Zhang, G. J., & McPhaden, M. J. (1995). The Relationship between Sea Surface Temperature and Latent Heat Flux in the Equatorial Pacific. *Journal of Climate*, *8*(3), 589–605.

THE PRESENT RESEARCH WORK HAS BEEN (PREPARED TO BE) PUBLISHED IN:

This research is being prepared to be published in a peer-review journal (the journal is not yet decided).